Two basic uncertainties affect our interpretation. First, not all Isua samples have high apparent initial $\varepsilon_{^{143}Nd}$ values. A range from about 0 to +3 is observed for other lithologies at Isua[2,3]. As shown in Fig. 3, reservoir ages obtained for $\varepsilon_{^{143}Nd} < 3$ are limited by the age of the Solar System (~4.566 Gyr). Some of the variability in apparent initial $\varepsilon_{^{143}Nd}$ is likely to be due to metamorphic effects. Measurements of $\varepsilon_{^{142}Nd}$ on samples with a variety of apparent initial $\varepsilon_{^{143}Nd}$ values could resolve this issue. Second, $^{142}Nd/^{144}Nd$ in the Ndβ standard may not be equal to the bulk Earth value. New high-precision measurements of $\varepsilon_{^{142}Nd}$ in meteorites and young terrestrial basalts are required if we are to resolve this issue. □

Received 16 October; accepted 24 November 1992.

1. Jacobsen, S. B. & Wasserburg, G. J. *Earth planet. Sci. Lett.* **50,** 139–155 (1980).
2. Hamilton, P. J., O'Nions, R. K., Bridgwater, D. & Nutman, A. *Earth planet. Sci. Lett.* **62,** 263–272 (1983).
3. Jacobsen, S. B. & Dymek, R. F. *J. geophys. Res.* **93,** 338–354 (1988).
4. Jacobsen, S. B. & Wasserburg, G. J. *Earth planet. Sci. Lett.* **67,** 137–150 (1984).
5. Jahn, B. M. *et al. Precamb. Res.* **34,** 311–346 (1987).
6. Galer, S. J. G. & Goldstein, S. L. *Geochim. cosmochim. Acta* **55,** 227–239 (1991).
7. Jacobsen, S. B. *Geochim. cosmochim. Acta* **52,** 1341–1350 (1988).
8. Jacobsen, S. B. *Earth planet. Sci. Lett.* **90,** 315–329 (1988).
9. Lugmair, G. W. & Marti, K. *Earth planet. Sci. Lett.* **35,** 273–284 (1987).
10. Nyquist, L. E., Harper, C. L., Wiesmann, H., Bansal, B. & Shih, C.-Y. *Meteoritics* **26,** 381 (1991).
11. Nyquist, L. E., Wiesmann, H., Bansal, B., Shih, C. Y. & Harper, C. L. *Lunar planet. Sci.* **XXII,** 989–990 (1991).
12. Nyquist, L. E., Bansal, B., Wiesmann, H. & Shih, C.-Y. *Lunar planet. Sci.* **XXIII,** 1009–1010 (1992).
13. Prinzhofer, A., Papanastassiou, D. A. & Wasserburg, G. J. *Geochim. cosmochim. Acta* **56,** 797–815 (1992).
14. Lugmair, G. W. & Galer, S. J. G. *Geochim. cosmochim. Acta* **56,** 1673–1694 (1992).
15. Collerson, K. D., Campbell, L. M., Weaver, B. L. & Palacz, Z. A. *Nature* **349,** 209–214 (1991).
16. Jacobsen, S. B. & Wasserburg, G. J. *J. geophys. Res.* **84,** 7411–7427 (1979).
17. Baadsgaard, H. *et al. Earth planet. Sci. Lett.* **68,** 221–228 (1984).
18. Harper, C. L. & Jacobsen, S. B. *Lunar planet. Sci.* **XXIII,** 487–488 (1992).
19. Bowring, S. A., Williams, I. S. & Compston, W. *Geology,* **17,** 971–975 (1989).
20. Black, L. P., Williams, I. S. & Compston, W. *Contrib. Miner. Petrol.* **94,** 427–437 (1986).
21. Liu, D. Y., Nutman, A. P., Compston, W., Wu, J. S. & Shen, Q. H. *Geology* **20,** 339–342 (1992).
22. Compston, W. & Pidgeon, R. T. *Nature* **321,** 766–769 (1986).
23. Froude, D. O. *et al. Nature* **304,** 616–618 (1983).
24. Maas, R. & McCulloch, M. T. *Geochim. cosmochim. Acta* **55,** 1915–1932 (1991).

ACKNOWLEDGEMENTS. This work was supported by the NSF and NASA.

TABLE 1 Mean laser-fusion $^{40}Ar/^{39}Ar$ dates for Konso Tephras

Sample number	Grain size (mm)	Grains (*n*)	Ca/K (Ave)	Ca/K ±	Age (Myr)	± (Myr)
24-91	1.0	10	0.162	0.176	1.34	0.04
16-91	1.0	10	0.046	0.071	1.38	0.07
1A-91	1-2	16	0.041	0.061	1.37	0.03
1B-91	1.0	10	0.028	0.034	1.35	0.02
Chari Tuff*	1-1.5	8	0.047	0.018	1.34	0.02
6015-03	*1-1.5*	*1*	*0.007*		*1.75*	*0.13*
6015-06	*1-1.5*	*1*	*0.009*		*1.48*	*0.01*
Chari Tuff†	1.0	6	0.063	0.048	1.38	0.02
6018-02	*1.0*	*1*	*0.421*		*1.52*	*0.02*
6018-03	*1.0*	*1*	*1.102*		*1.94*	*0.02*
6018-07	*1.0*	*1*	*0.130*		*1.62*	*0.01*
6018-10	*1.0*	*1*	*1.516*		*2.61*	*0.06*
T-1	1.0	11	0.014	0.017	1.444	0.01
19-91	0.5	5	0.014	0.024	1.44	0.05
4A-91	1.0	8	0.114	0.078	1.66	0.03
4B-91	1.0	4	0.020	0.023	1.87	0.04
6-91	0.5	2	0.016	0.023	1.84	0.12
KBS Tuff‡	1.0	10	0.050	0.026	1.895	0.01

Grain size (mm) is given for the average maximum dimension of the feldspar population. *n* is the number of single-grain laser-fusion measurements. Ca/K, an average and standard deviation of *n* grains, is derived by multiplying the measured $^{37}Ar/^{39}Ar$ ratio of each grain by 1.96. The mean age and error (±1 s.d.) are weighted mean values derived from the single-grain results, and are computed using an inverse variance weighting factor that uses deviations about a weighted mean to determine the weighted error[29,30]. Individual grain errors (not shown) reflect errors in *J* (an irradiation parameter) and in the determination of Ar isotopic ratios, which in turn propagate errors in discrimination and errors in Ar beam intensities from sample and blank[29]. Data in italics are excluded from the mean age. Samples of the Chari and KBS Tuffs were collected and provided by Garniss H. Curtis: Chari Tuff*, GHC-815; Chari Tuff†, GHC-818; and KBS Tuff‡, ER 131-0001. Clear, euhedral feldspars from the coarsest sieve fraction were hand-picked and irradiated for 0.5 h at 8 MW at the Omega West research reactor of the Los Alamos National Laboratory, which has a fast neutron fluence of 5.7×10^{13} n cm^{-1} s^{-1}. Cadmium shielding was used to reduce the thermal neutron production of ^{40}Ar. After irradiation, samples were transferred to a copper holder and loaded onto the extraction line for overnight bakeout at ~200 °C. Single grain samples are fused with an 8 W argon-ion laser. Abundances of the Ar isotopes are measured on a MAP-215 noble gas mass spectrometer fitted with a Balzers electron multiplier operating at a gain of about 20,000. The volume of a typical sanidine grain measured in this study is $\sim 1 \times 10^{-3}$ cm^3, corresponding to a sample mass of 3 mg per grain. Typical system blank volumes of ^{40}Ar, ^{39}Ar, ^{38}Ar, ^{37}Ar and ^{36}Ar are 4, 2, 0.08, 0.3, and 0.3×10^{-17} mol, respectively. Neutron fluence monitor and constants as in ref. 6. Detailed results for individual grain analyses are available from R.C.W. by request.

The earliest Acheulean from Konso-Gardula

Berhane Asfaw*, Yonas Beyene*, Gen Suwa†, Robert C. Walter‡, Tim D. White§, Giday WoldeGabriel‖ & Tesfaye Yemane¶

* Palaeoanthropology Laboratory, Ministry of Culture, PO Box 5717, Addis Ababa, Ethiopia
† Department of Anthropology, University of Tokyo, Bunkyo-ku, Hongo, 113 Tokyo, Japan
‡ Geochronology Center, Institute of Human Origins, 2453 Ridge Road, Berkeley, California 94709, USA
§ Laboratory for Human Evolutionary Studies, Department of Anthropology, University of California, Berkeley, California 94720, USA
‖ EES-1/D462, Los Alamos National Laboratory, Los Alamos, New Mexico 87545, USA
¶ Department of Earth Sciences, Iowa State University, Ames, Iowa 50011, USA

KONSO-GARDULA is a palaeoanthropological area discovered by the 1991 Palaeoanthropological Inventory of Ethiopia[1–5] in the southern Main Ethiopian Rift. The Konso-Gardula sediments span the period about 1.3–1.9 million years ago. They contain rich Acheulean archaeological occurrences. Vertebrate fossils include early *Homo*.

Konso-Gardula (KGA) is on the western flank of the rift in the Segen River's headwaters north of Konso town (Fig. 1). Precambrian basement and >50 m of Plio-Pleistocene deposits are exposed across 12 × 5 km between 1,200 m and 1,400 m altitude. The local dip of Plio-Pleistocene strata approximates local drainage, providing wide spatial exposure of these conglomerates, sands and gravels, silts, dark brown clays and interbedded volcanic tuffs.

Laser-fusion $^{40}Ar/^{39}Ar$ dating studies[6,7] were done on KGA and Turkana Basin[8] rocks (Table 1). Analyses of these tephras yield dates of 1.34, 1.38 and 1.36 million years (Myr), respectively, and two samples of the Chari Tuff yield dates of 1.34 and 1.38 Myr. These results suggest that 1.36 ± 0.02 Myr is an accurate estimate of the Chari Tuff's age and that these Konso tuffs are temporally equivalent with the Chari Tuff at Koobi Fora.

In locality KGA 4E, tephra 19-91 is 3-5 m above a hominid molar, and is dated to 1.44 ± 0.05 Myr. An equivalent unit (Tuff T−1) located ~500 m north is dated to 1.44 ± 0.01 Myr. Tuffs in fault-bounded outcrops sampled near the western fault contact of the Konso beds date to 1.66 ± 0.03 (4A-91) and 1.87 ± 0.04 (4B-91) Myr. The oldest tephras at Konso are thus within errors of the KBS Tuff, which is dated here to 1.895 ± 0.011 Myr (Table 1).

The Acheulean was unknown in southern Ethiopia before the discovery of KGA. Stone tools are abundant and diverse, par-

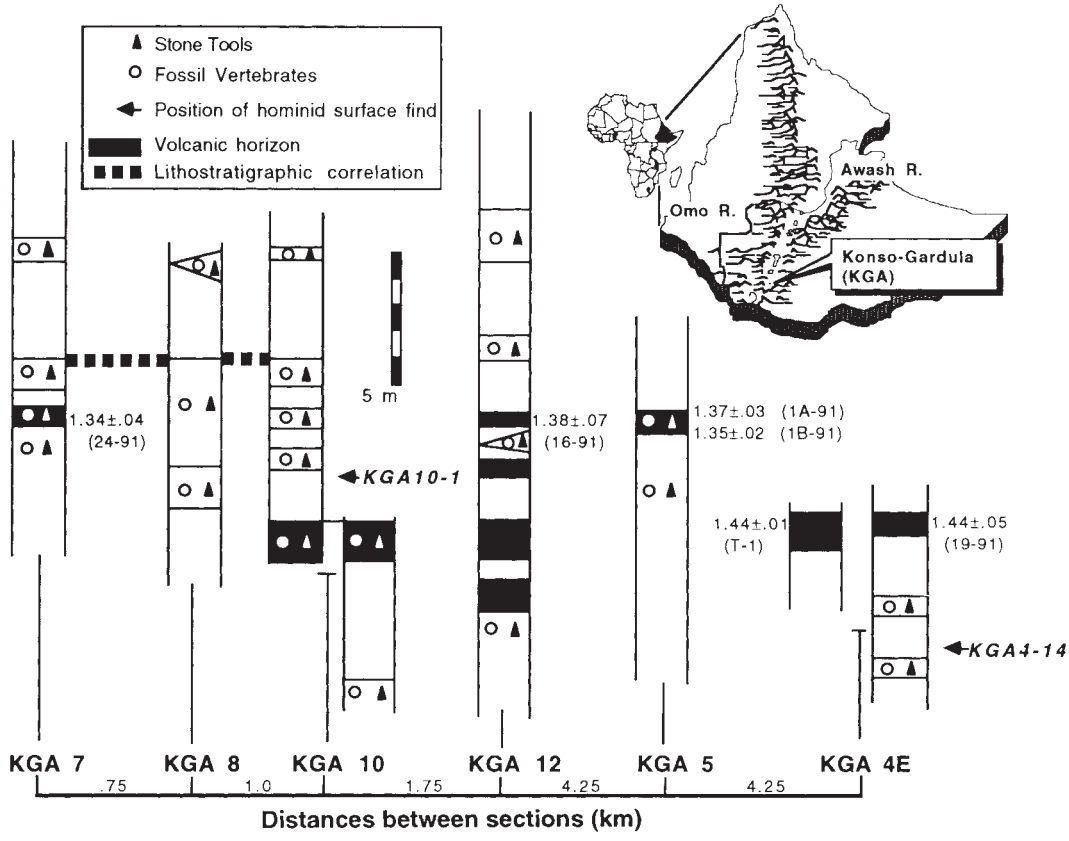

FIG. 1 Stratigraphic and geometric relationships between the dated volcanic horizons, fossil vertebrate remains, and *in situ* archaeological occurrences at the main KGA localities. Transects across outcrops of KGA sediments intercepted archaeological and faunal remains. Localities and sample locations were mapped on aerial photos and by GPS placement. Hominid surface finds were assessed in the field to have derived from the local outcrops depicted here (based on fragment scatter and preservation style).

ticularly in strata immediately above and below the tuff dated to 1.34–1.38 Myr. Archaeological and palaeontological remains are concentrated in thin (10 cm) sand lenses to thicker sand and silt strata (Fig. 1). Many vertical outcrops reveal artefacts and fossils *in situ*, often densely concentrated. Evidence of fluviatile transport common in other Acheulean assemblages[9–11] is absent. Tools were made from basalt, quartz, quartzite and silicic volcanic rock.

The pooled tool assemblage from KGA 3, 5 and 7–12 is dominated by roughly made bifaces and trihedral picks from cobbles, blocks, cores and flakes. Bifaces often display cortical butt and deep oblique flake scars. Some bifaces and picks attain great length ($268 \times 240 \times 70$ mm handaxe; $270 \times 75 \times 67$ pick), but basic morphology of type tools is constant over a wide size range. Flakes are generally untrimmed, with a virtual absence of typologically diversified, retouched tools. Cleavers are rare and spheroids absent. Typologically, these assemblages best match those from middle Bed II at Olduvai (EF-HR, SHK; ref. 9).

The KGA artefacts are closely associated to fossilized bones. Evidence of hominid-induced modification of large mammal bones includes percussion pits and striae, internally conchoidal flake scars and cutmarks. Palaeontological resources are rich; fossils were observed in all KGA localities. Excellent bone preservation will enhance archaeological investigation of *in situ* assemblages. Biochronological placement of the vertebrate fauna (Table 2) is consistent with the radiometric dates.

A hominid upper third molar and a nearly complete left mandible with condyle and P_4–M_3 were recovered from KGA. Two[12], and possibly three[13,14] early hominid species are recorded in contemporary rocks of the Turkana Basin and Olduvai: *Australopithecus boisei* and *Homo erectus*. Both 1991 KGA hominid specimens are attributed to *Homo* because they lack specialized characters[13] of robust *Australopithecus*. The mandible is morphologically and metrically similar to *Homo erectus* specimens (for some, *Homo ergaster*[13]), particularly KNM-ER 992. As in other early African *H. erectus*, the KGA 10-1 mandible has a very robust corpus (Fig. 2). The M_3 is distinctly smaller than M_1 in the $M_2 > M_1 > M_3$ size sequence. The M_1 shape index does not exhibit the buccolingual narrowing of *H. habilis* counterparts. The M_3 wear pattern has an exaggerated distolingual component, as in KNM-ER 730. Molars show a low level of root bifurcation as in KNM-ER 992. Interproximal grooves between all mandibular teeth probably indicate modification by toothpick[15] or sinew[16] manipulation. This is among the largest of the still limited sample of early Arican *H. erectus* mandibles[13]. It is too large for a cranium the size of KNM-ER 3733 and could be a better size match for the OH 9 cranium.

Biological and technological dynamics involved in the origin of the Acheulean and the origin and early evolution of *H. erectus* are poorly understood. Olduvai and west Natron localities were previously considered the earliest evidence of the Acheulean. Because only Bed I has yielded reliable radiometric dates[6], the ages of these early Acheulean sites were poorly constrained. The KGA results supplement precise Ar/Ar dating results at Olorgesailie[17,18] and Kesem-Kebena[4] to demonstrate great antiquity for the Acheulean. It appears abruptly in eastern Africa at 1.4 Myr, following a million years of exclusively Oldowan occurrences[19]. Compared to these, the Acheulean's earliest manifestation at KGA shows surprising control over raw material and tool form. The temporal stability of the Acheulean industrial complex is thereby emphasized. Also surprising is the spectacular abundance of KGA artefacts and the apparently intensive Lower Pleistocene occupation of this basin. Contemporary deposits in the nearby Turkana Basin (>200 km away) yielded many hominid fossils, but definitive Acheulean assemblages are lacking at Koobi Fora[20]. This difference may relate to the close proximity of raw material sources to the KGA discard loci.

Leakey attributed the origin of the Acheulean at Olduvai to immigrant *Homo erectus*[9]. Subsequent discovery of terminal

TABLE 2 Faunal list for selected Konso-Gardula localities

Taxa	KGA locality 3	4E	4W	5	6	7	8	10	11	12
Elephantidae										
Elephas recki recki						•				
Elephas recki recki/ileretensis	•	•	•	•			•	•	•	•
Rhinocerotidae										
Ceratotherium simum	•			•						•
Equidae										
Hipparion libycum		•								•
Equus cf. oldowayensis	•	•	•	•		•	•	•		•
Hippopotamidae										
Hippopotamus/Hexaprotodon sp	•	•	•	•	•	•	•	•	•	•
Suidae										
Kolpochoerus majus		•	•	•					•	
Kolpochoerus olduvaiensis			•					•		
Metridiochoerus modestus	•					•				•
Metridiochoerus hopwoodi						•	•	•		•
Metridiochoerus compactus								•		
Giraffidae										
Sivatherium sp.		•		•						
Giraffa sp.			•			•				
Bovidae										
Tragelaphus cf. scriptus								•		
Tragelaphus strepsicerus								•		
Reduncini	•	•	•	•	•	•	•	•		•
Kobus sp.								•		
Kobus cf. sigmoidalis			•							
Bovini	•	•	•	•		•	•	•	•	•
Hippotragus sp.								•		
Damaliscus sp.			•							
Damaliscus niro							•	•		
Parmularius angusticornis								•		
Connochaetes sp.								•		
Alcelaphini	•	•	•	•		•	•	•	•	•
Antilopini		•		•						
Gazella						•			•	
Aepyceros			•					•		
Primates										
Papio sp.								•		
Theropithecus oswaldi			•							
Homo sp.		•								
Homo erectus								•		
Carnivora										
Dinofelis sp. aff. *piveteaui*		•						•		
Hyaenidae		•						•		
Reptilia										
Python										•
Crocodylus sp.	•	•		•	•	•	•			
Chelonia	•	•			•	•				
Aves		•								
Pisces	•									

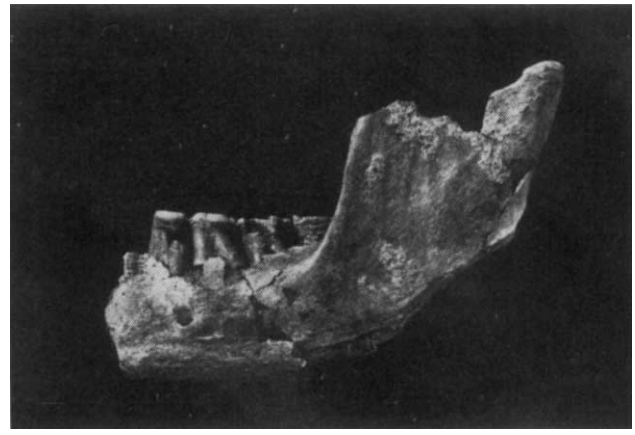

FIG. 2 Lateral view of the KGA 10-1 hominid mandible, attributed to *Homo erectus*.

Pliocene (1.7 Myr) *H. erectus*[21] broadens its temporal and anatomical ranges (prompting some to recognize a new species for these early African remains, *H. ergaster*)[13,14]. Discoveries at Olduvai and Turkana demonstrate close temporal proximity of *H. habilis* and early African *H. erectus*, but shed little light on the evolutionary relationships (punctuational or cladistic; *in situ* or allopatric) between the still inadequately sampled populations.

H. erectus was contemporary with the Acheulean at KGA and continued to be associated with it long after the subsequent extinction of other hominid lineage(s). The recent discovery of a possibly early Pleistocene hominid mandible at Dmanisi[22] is a reminder of the still inadequate Eurasian early hominid record. Despite repeated claims to the contrary, well dated Eurasian evidence of occupation is unknown before ~1.0–1.4 Myr. The preponderance of the evidence is that *H. erectus* made its evolutionary appearance in Africa sometime before 1.7 Myr and dispersed into Eurasia within the next 0.3–0.5 Myr, at some point carrying the Acheulean. But the evidence is largely African, and the scope of appropriate deposits in intensively studied areas of southern Eurasia is limited. This combines with the lack of palaeoanthropological exploration in large parts of southern Eurasia to preclude definitive conclusions about the timing and direction of early hominid movements.

The last decade witnessed a proliferation of attempts to causally link hominid evolutionary events to changes in global climate[23–25] (but for cautionary views, see refs 26, 27). Vrba[24] suggests that "... changes to open and arid conditions may have triggered the origin of *H. erectus* and of his characteristic tool kit ...", and that "the period around 0.9 Myr may also coincide with the earliest massive geographic expansion of any hominid species, namely *H. erectus*" (p. 421). The first African records of this taxon and the Acheulean, however, are now set solidly at 1.7 and 1.4 Myr, respectively. These appearances substantially postdate the global cooling between 2.4 and 2.8 Myr (ref. 28). The probable dispersal of *H. erectus* and the Acheulean from Africa into Eurasia substantially predates pronounced changes in global ice budget between 0.9 and 0.7 Myr. The period between 1.8 and 1.4 Myr was unmarked by major global climatic changes of comparable degree, but witnessed profound changes in hominid anatomy and technology. Research at early African occurrences like Konso-Gardula is needed to understand these changes. □

Received 24 June; accepted 27 October 1992.

1. Asfaw, B., Ebinger, C., Harding, D., White, T. & WoldeGabriel, G. *Nat. Geogr. Res.* **6,** 418–434 (1990).
2. Asfaw, B. *et al. J. hum. Evol.* **21,** 137–143 (1991).
3. Suwa, G., White, T., Asfaw, B., WoldeGabriel, G. & Yemane, T. *Palaeont. afr.* **28,** 23–28 (1991).
4. WoldeGabriel, G. *et al. J. Field Archaeol.* **19,** (in the press).
5. WoldeGabriel, G., Yemane, T., Suwa, G., White, T. & Asfaw, B. *J. Afr. Earth. Sci.* **13,** 437–447 (1991).
6. Walter, R. C., Manega, P. C., Hay, R. L., Drake, R. E. & Curtis, G. H. *Nature* **354,** 145–149 (1991).
7. Walter, R. C., Manega, P. C. & Hay, R. L. *Quat. Int.* **13/14,** 37–46 (1992).
8. McDougall, I. *Geol. Soc. Am. Bull.* **96,** 159–175 (1985).
9. Leakey, M. D. *Olduvai Gorge. Volume 3: Excavations in Beds I and II, 1960–1963* (Cambridge Univ. Press, Cambridge, 1971).
10. Chavaillon, J. & Piperno, M. *Bull. Soc. préhist. Fr.* **72,** 134–138 (1975).
11. Clark, J. D. & Kurashina, H. *Nature* **282,** 33–39 (1979).
12. Tobias, P. V. *Olduvai Gorge Project IV: The Skulls, Endocasts and Teeth of* Homo Habilis (Cambridge Univ. Press, Cambridge 1991).
13. Wood, B. A. *Koobi Fora Research Project IV: Hominid Cranial Remains from Koobi Fora* (Clarendon, Oxford, 1991).
14. Wood, B. A. *Nature* **355,** 783–790 (1992).
15. Formicola, V. *Am. J. phys. Anthrop.* **86,** 85–86 (1991).
16. Brown, T. & Molnar, S. *Am. J. phys. Anthrop.* **81,** 545–553 (1990).
17. Bye, B. A., Brown, F. H., Cerling, T. E. & McDougall, I. *Nature* **329,** 237–239 (1987).
18. Deino, A. & Potts, R. *J. Geophys. Res.* **95,** 8453–8470 (1990).
19. Clark, J. D. *The Prehistory of Africa* (Praeger, New York, 1970).

20. Isaac, G. L. & Harris, J. W. K. in *Koobi Fora Research Project Volume I: The Fossil Hominids and an Introduction to their Context, 1968–1974* (eds Leakey, R. E. & Leakey, M. G.) 64–85 (Clarendon, Oxford, 1978).
21. Feibel, C. S., Brown, F. H. & McDougall, I. *Am. phys. Anthrop.* **78,** 595–622 (1989).
22. Dzaparidze, V. *et al. Jahrb. Röm.-Germ. Zentralmus. Mainz* **36,** 67–116 (1989).
23. Brain, C. K. *Ann. geol. Soc. S. Afr.* **84,** 1–19 (1981).
24. Vrba, E. S. in *Evolutionary History of the 'Robust' Australopithecines* (ed. Grine, F. E.) 405–426 (Aldine de Gruyter, New York, 1988).
25. Hill, A. *et al. Nature* **355,** 719–722 (1992).
26. Hill, A. *J. hum. Evol.* **16,** 583–597 (1987).
27. White, T. D. in *Evolutionary History of the 'Robust' Australopithecines* (ed. Grine, F. E.) 449–483 (Aldine de Gruyter, New York, 1988).
28. Prentice, M. L. & Denton, G. H. in *Evolutionary History of the 'Robust' Australopithecines* (ed. Grine, F. E.) 383–403 (Aldine de Gruyter, New York, 1988).
29. Deino, A., Tauxe, L., Monaghan, M. & Drake, R. *J. Geol.* **98,** 567–587 (1990).
30. Samson, S. D. & Alexander, E. C. *Chem. Geol. (Iso. Geosci.)* **66,** 27–34 (1987).

ACKNOWLEDGEMENTS. We thank A. Ademasu, T. Hagos, T. Wodajo and Y. Haile-Selassie for field discoveries, W. Abomssa, the National Museums of Ethiopia, and Kenya and A. Getty for access to comparative materials, J. D. Clark and F. C. Howell for guidance and G. Curtis and R. C. Drake for assistance with dating samples. The Palaeoanthropological Inventory is a project of the Ethiopian Ministry of Culture and Sports Affairs, supported by the Committee for Research and Exploration of the National Geographic Society, with additional funding from the Wenner Gren Foundation for Anthropological Research, the Anthropology Program of the National Science Foundation, the Japan Society for Promotion of Science, the University of California Collaborative Research Program of the Institute of Geophysics and Planetary Physics at Los Alamos National Laboratory, and Magellan.

Mitotic domains in the early embryo of the zebrafish

Donald A. Kane*, Rachel M. Warga* & Charles B. Kimmel

Institute of Neuroscience, University of Oregon, Eugene, Oregon 97403, USA

AT the midblastula transition in the zebrafish, three, and only three, spatially separate mitotic domains arise with distinctive cycle lengths and rhythms. As in *Drosophila*[1] and at about the equivalent stage, the mitotic domains reflect the fate map, but they do so only very crudely: two are extraembryonic and the third forms the entire embryo. The domains appear not to subdivide during gastrulation, when the germ layers form and when cells probably commit to their eventual fates. The domains may signal specification of morphogenesis rather than cell fate, because, shortly after they appear, each assumes a different role during epiboly, the first morphogenetic movement of the embryo. During meroblastic cleavage, and continuing in the early blastula, zebrafish blastomeres divide rapidly and synchronously. At the time of the tenth cleavage, the beginning of the midblastula transition, the cell cycle lengthens, and, as in *Xenopus*[2] and *Drosophila*[3], cycle length comes under nucleocytoplasmic control (D.A.K. and C.B.K., manuscript in preparation). This nucleocytoplasmic control seems to be maintained during cycle lengthening in the next 2 or 3 cycles, comprising a midblastula transition period. We now show that functionally distinct subsets of cells that arise during this period have reproducibly different mitotic cycle lengths.

There are three of these domains, and they can be recognized morphologically (Fig. 1*a* and *b*). Two are of blastoderm cells, an outer enveloping monolayered epithelial layer (EVL), and an inner, or 'deep' mass of spherical cells. The third is the single giant multinucleate yolk cell; its syncytium of non-yolky cytoplasm and nuclei, the yolk syncytial layer (YSL), immediately underlies the marginal rim of the blastoderm[4,5]. Video time-lapse analysis reveals that, during the midblastula transition (MBT) period, average mitotic cycle lengths within the domains diverge (Fig. 1*c*), YSL nuclei dividing most rapidly, and EVL cells most slowly.

Cell-lineage analysis (Fig. 2) readily distinguishes the domains, not only by mitotic cycle length, but also according to division synchrony. Examining single lineages that split into separate domains sensitively demonstrates the origins of the cycle-length differences, indicated as 'mitotic borders' in Fig. 2*c* and *d*. Cycle lengths diverge rapidly upon the lineage segregation; for example in Fig. 2*c*, YSL nuclei divide more rapidly than their deep cell cousins as soon as the YSL forms at cycle 11. Similarly, in Fig. 2*d*, segregation of sister cells into the EVL and deep domains occurs after cycles 9 and 11, and the deep cells immediately divide more rapidly than their EVL sisters.

During the MBT period there is a close correlation between cycle lengths of daughter cell pairs with that of their mother (Fig. 3*a*–*c*). This is expected if control is by the nucleocytoplasmic ratio, for, if one assumes no growth during these divisions, the total volume of the daughters will equal that of the mothers. Then, beginning with daughters born in the late blastula, 4 h postfertilization, the mother–daughter correlation weakens, suggesting an end to the MBT period. In the deep domain, the cell cycle of the daughters becomes shorter than expected in late cycle 13 and cycle 14 (plateau in Fig. 3*a*). Afterwards, as deep

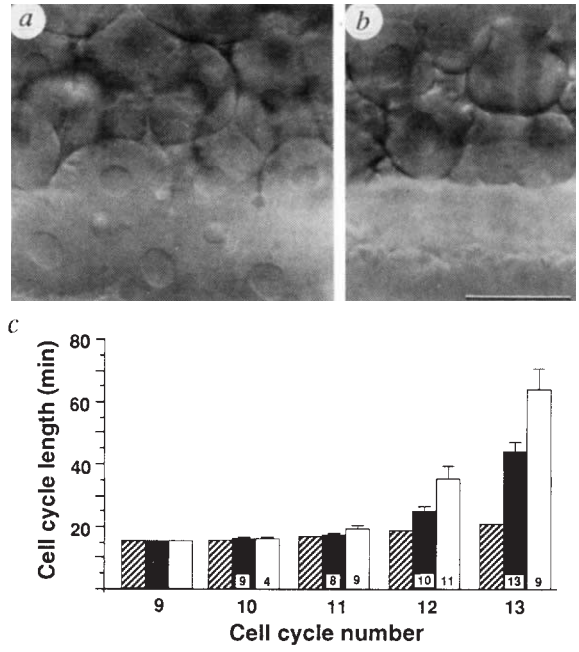

FIG. 1 Mitotic domains are evident during zebrafish MBT, from cycle 10 to 12. Note that cycle-10 corresponds to the 512-cell stage of ref. 10. *a*, Photomicrograph of the enveloping layer (EVL) of the blastoderm (cells in top half of photograph) and yolk syncytial layer (YSL) of the yolk cell (nuclei at bottom) at cycle 12. *b*, Photomicrograph of the deep cells (cells in top half of photograph) and yolk cell (bottom) at cycle 12, in a focal plane 20 μm beneath *a*. Note spherical shape of the deep cells compared to the epithelial appearance of the overlying EVL cells. Scale bar for *a* and *b*, 30 μm. *c*, Average cycle length of the mitotic domains, comparing the three mitotic domains of one embryo. Cycle 9 is typically the last synchronous short cycle (D.A.K. and C.B.K. submitted). Although the magnitude and initiation of the lengthening varied between embryos, all embryos had statistically significant differences ($P < 0.05$) between domains by cycle 12. Symbols: diagonal pattern, YSL; solid bars, deep cells; clear bars, EVL. Numbers in the bars (except for the YSL, which is part of a single cell) indicate the number of cells measured; error bars indicate the s.e.m.
METHODS. Eggs were collected from spawning zebrafish within 1.5 h of the time of fertilization, dechorionated, and monitored to verify the early staging of the eggs. Lineage analysis was done according to ref. 21 using 5 mg ml^{-1} tetramethylrhodomaine-isothiocyanate dextran (Molecular Probes, Oregon) in 0.2 M KCl as the lineage dye. Observations were made with a Zeiss Universal microscope equipped with a Leitz 50× water-immersion objective and a computer-controlled stage using Nomarski optics and ultraviolet epilumination (D.A.K. and C.B.K., submitted). Recording and playback for time-lapse was controlled by a Macintosh II computer (Apple Computer Company) equipped with a Quick Capture board and RasterOps board running software Neuro Video 3.0 (ref. 22) and recording video images onto an Optical Memory Disk Recorder (Panasonic).

* Present address: Max-Planck-Institut für Entwicklingsbiologie, Spemannstrasse 35/II, D-7400 Tübingen, Germany.